α-γ transition in Ce: A detailed analysis of electron spectroscopy

L. Z. Liu* and J. W. Allen
Randall Laboratory of Physics, The University of Michigan, Ann Arbor, Michigan 48109-1120

O. Gunnarsson, N. E. Christensen,† and O. K. Andersen
Max-Planck-Institut für Festkörperforschung, D-7000 Stuttgart 80, Federal Republic of Germany
(Received 29 July 1991)

Impurity Anderson Hamiltonian parameters have been obtained for the α and γ phases of Ce by a detailed analysis and a comparison with the published electron spectroscopy data, using the $1/N$ expansion theory with energy-dependent hybridization calculated in the local-spin-density-functional approximation. With the surface contributions included, the theory provides a remarkably good description of various spectroscopic data with the same set of Hamiltonian parameters for all spectroscopies. The calculated susceptibility for these parameters is in good agreement with the experimental value. A previous result of analyzing the valence-band spectrum gave a susceptibility value that is much too large compared with the experimental one. We find that this discrepancy is caused by ignoring the surface emission in the spectral analysis.

I. INTRODUCTION

Ce metal is an archetypal material in the study of strongly interacting f-electron systems. It has a complex phase diagram,[1] involving different lattice structures, and varying magnetic and superconducting behaviors. This rich variety in properties is generally taken to be related to the $4f$ electrons in the element. The most fascinating property of Ce metal is the occurrence of the α-γ isostructural (fcc to fcc) solid-solid phase transition, which ends in a critical point, analogous to the well-known liquid-gas phase transition. In this, Ce is unique among elemental solids. The high-temperature γ phase displays a Curie-Weiss-like magnetic behavior, implying the existence of local magnetic moments, while the α phase has a Pauli-like paramagnetic behavior with the cell volume collapsed by about 15%. There are also many Ce intermetallic compounds which mimic one or the other of the two phases.

The nature of the α-γ phase transition in Ce, and of the α-like and γ-like behavior of Ce compounds, has been the subject of debate for the past 40 years. It is only during the past decade, largely due to the interpretation and understanding of the new results of photoemission (PES) and Bremsstrahlung isochromatic (BIS) spectroscopy of $4f$ electrons and the x-ray photoemission spectroscopy (XPS) of the $3d$ core electrons in Ce materials, that a unified understanding of both the spectral and low-energy properties of these materials has been achieved.[2] Of particular importance to the development was the use of the Kondo aspects of the Anderson impurity Hamiltonian[3] (AIH) to provide a basis for the Kondo volume collapse (KVC) model,[4] which gives a semiquantitative explanation of the α-γ transition in Ce metal. The next important advance was the application of the $1/N$ expansion[5-7] to the AIH. This theory provides a systematic method for calculating the various electron spectra and ground-state quantities for the AIH. The theory has been used to analyze spectroscopic data to obtain AIH parameters, and then to calculate values of low-energy properties like the magnetic susceptibility. These spectroscopically derived values are in fair agreement with values obtainable directly from experiment, and it has been found that all known Ce intermetallics are in the Kondo regime of the AIH.[8] Another theoretical advance[9-11] has been first-principles local-density-functional approximation (LDA) calculations of the AIH parameters, which agree reasonably well with the spectroscopically measured parameters.

In spite of its paradigmatic importance, and the fact that a large number of $4f$ PES/BIS and $3d$ XPS data[12-16] are available, including beautiful high-resolution valence-band spectra, there has been no detailed consistent AIH analysis for α- and γ-Ce. The only analysis of the high-resolution valence-band spectra[16] implies magnetic susceptibility values that are four times larger than the experimental ones, a discrepancy so large as to invalidate the KVC model. With the ultimate goal of making a parameter-free quantitative examination of the KVC model, we have undertaken to compare and analyze all the spectroscopic data for α- and γ-Ce.

In the course of this work we have found it essential to include in the analysis the effect of an altered valence at the surface. This is especially important for the valence-band PES, which involves electrons of lower kinetic energies than that for BIS and for $3d$ XPS, and is thus more surface sensitive. A recent experimental study[17] for α-like Ce compounds provides direct evidence of these surface effects and shows that even at Ce $3d$ XPS photoelectron kinetic energies ($\sim$600 eV with Al $K\alpha$ source) surface emission cannot be neglected in quantitative analysis of the spectra.

In this paper, we present the results of a detailed comparison and analysis of published $4f$ PES/BIS and $3d$ XPS spectra of α- and γ-Ce using the $1/N$ theory for the AIH with an energy-dependent hybridization calculated

from the LDA.[9] Surface contributions to the various spectra are included. The zero-temperature susceptibility $\chi(0)$ calculated for parameters obtained from the spectroscopy analysis is in good agreement with the experimental value. We find that the serious discrepancy between ground-state properties and the results of the earlier analysis[16] of the high-resolution valence-band data is removed by including the surface contribution in the spectral analysis. Results from a KVC calculation based on the spectroscopic AIH parameters are presented in a subsequent paper.[18]

II. THEORETICAL TREATMENT

The theoretical treatment is based on a generalized AIH:

$$H=\sum_{\nu=1}^{2}\sum_{m=-j_\nu}^{j_\nu}\left[\int d\varepsilon\,\varepsilon\psi^\dagger_{\nu m\varepsilon}\psi_{\nu m\varepsilon}+[\varepsilon_{f\nu}+(1-n_c)U_{f_c}]\psi^\dagger_{\nu m}\psi_{\nu m}+\int d\varepsilon[V(\varepsilon)\psi^\dagger_{\nu m}\psi_{\nu m\varepsilon}+\text{H.c.}]+\frac{U}{2}\sum_{\nu',m'\neq\nu,m}n_{\nu m}n_{\nu' m'}\right]. \quad (1)$$

The first three terms of the Hamiltonian represent the conduction-band states, the N-fold degenerate f state, and the hopping between these states. The spin-orbit splitting of the f level is included, with energies ε_f and $\varepsilon_f+\Delta\varepsilon_f$ for the j values equaling $\frac{5}{2}$ and $\frac{7}{2}$. The fourth term describes the Coulomb interaction energy U between two f electrons. The influence of a core hole on the f electrons is included in the second term as an attractive energy U_{fc}. The calculations have been performed to second order in the $1/N$ expansion approach, with basis states including the lowest order f^0, f^1, and f^2, and the second-order f^0 states.[6,7] The hopping matrix element $V(\varepsilon)$ used in this study has been calculated[9] from the local spin-density approximation of the density-functional formulism. Figure 1 shows the calculated hybridization strength $\pi|V(\varepsilon)|^2$ for both α- and γ-Ce. The projected density of states of the $4f$ and conduction states ($6s$, $6p$, ad $5d$) of α-Ce are also shown in the figure. $|V(\varepsilon)|^2$ can be interpreted as the product of the conduction density of states $\rho(\varepsilon)$ and an average hopping matrix element squared $|v(\varepsilon)|^2$:

$$|V(\varepsilon)|^2=\rho(\varepsilon)|v(\varepsilon)|^2 . \quad (2)$$

As shown in the figure, the major features of $\rho(\varepsilon)$ are reflected in $|V(\varepsilon)|^2$. This hybridization is f-configuration dependent, and is calculated for the f^1 configuration since this is the most important one for Ce. In order to fit the spectra, we have to rescale $V(\varepsilon)$ by a factor κ, i.e.,

$$V(\varepsilon)\rightarrow\kappa V(\varepsilon) . \quad (3)$$

The origin of κ will be discussed below.

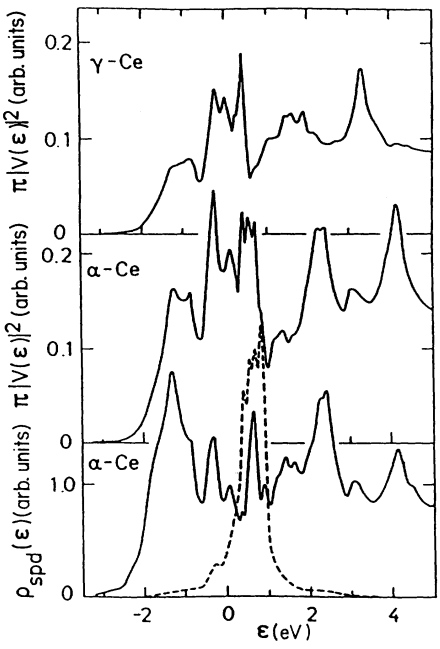

FIG. 1. The hybridization strength $\pi|V(\varepsilon)|^2$ for α- and γ-Ce calculated from local spin-density approximation. The lower panel of the figure shows the projected density of states of the f (dashed lines) and conduction ($6s$, $5p$, $6p$) states (solid lines).

III. SPECTROSCOPY DATA

In order to examine the uniqueness and consistency of the experimental data, we have digitized and compared the various spectroscopy measurements published by different authors as shown in Fig. 2. For α-Ce, there is only one published BIS spectrum in the literature. The two sets of γ-phase BIS spectra[13,15] are found to be essentially identical. For both phases, there are two valence-band PES (VBPES) studies at different resolution. The middle panel of Fig. 2 compares the spectra taken at photon energy 40 eV. In order to make an appropriate comparison, the higher-resolution data set[16] (dotted curve) has been convolved with a Gaussian function to simulate the low-resolution data.[14] The inelastic background in these spectra have been subtracted from the raw data in such a way that the background is proportional to the convolution of the primary spectrum with the inelastic energy-loss spectrum, approximated by a step function.[8] We have found that the two sets of VBPES data for the α phase match well only if the low-resolution data has the energy scaled up by about 10% relative to the high-resolution one. The reason for having to do this is not clear. The two sets of VBPES data for the γ phase are consistent without scaling as shown in the figure. The inelastic backgrounds in the $3d$ XPS spectra in Fig. 2 are also removed using the same method as for the VBPES. For the α phase, there is only one published $3d$ XPS spectrum in the literature. It is apparent from the figure that the two spectra for the γ phase are consistent. Thus, overall, the comparison shows that the spectroscopy data from different authors are consistent. The solid-line spectra are used for our analysis.

The $4f$ PES spectra, shown in Fig. 3, have been extracted from VBPES spectra taken in the photon energy range 40 to 60 eV,[14] using the fact that the relative cross section of the $4f$ to valence band (mainly $5d$) increases rapidly in this energy range. The low-resolution data sets are used because they cover a wider energy range than the high-resolution one. This is the first quantitative extraction of a $4f$ spectrum from data taken in this particular energy range. We assume that interference between the $4f$ and valence-band electrons is negligible, and the $4f$ spectrum is then obtained by scaling and subtracting two spectra according to the $h\nu$ dependence of the $4f$ and $5d$ PES cross section derived empirically[19] from Pr and La PES data. From VBPES data available at 40, 50, and 60 eV, we can derive independently two sets of $4f$ PES spectra which are slightly different due, we assume, to the uncertainty in determining the cross sections. If we vary the ratio of the $5d$ to $4f$ cross sections at 50 and 60 eV by about 20%, the same for both the α and γ phases, then the two sets of $4f$ spectra are almost identical.

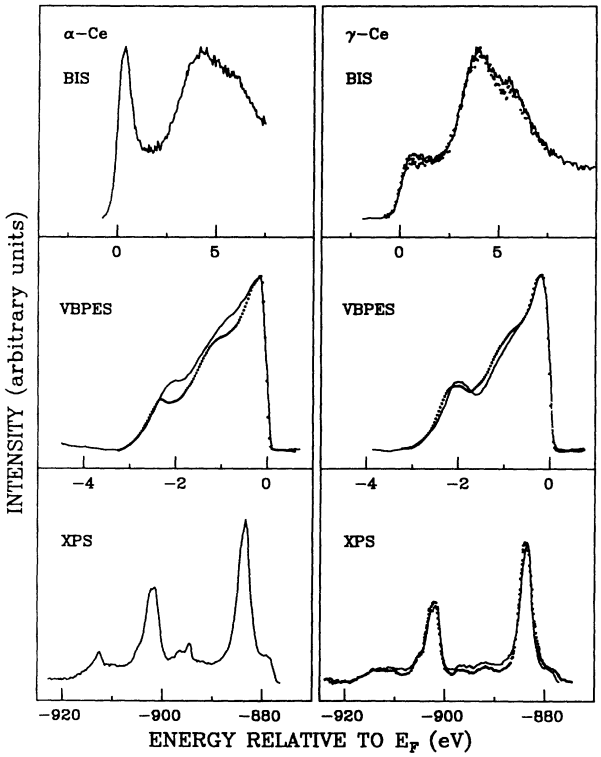

FIG. 2. Comparison of experimental BIS, VBPES, and $3d$ XPS spectra of α- and γ-Ce taken from different works. The left panel is for α-Ce, and the right panel is for γ-Ce. The high-resolution VBPES data (dotted lines) have been broadened in order to compare with the low-resolution data. References are α-Ce BIS: Ref. 13; VBPES: Ref. 14 (solid lines), Ref. 16 (dotted lines); $3d$ XPS: Ref. 13 (solid lines); γ-Ce BIS: Ref. 15 (solid lines), Ref. 13 (dotted lines); VBPES: Ref. 14 (solid lines), Ref. 16 (dotted lines); and $3d$ XPS: Ref. 13 (solid lines), Ref. 12 (dotted lines). Solid-line data are used for analysis.

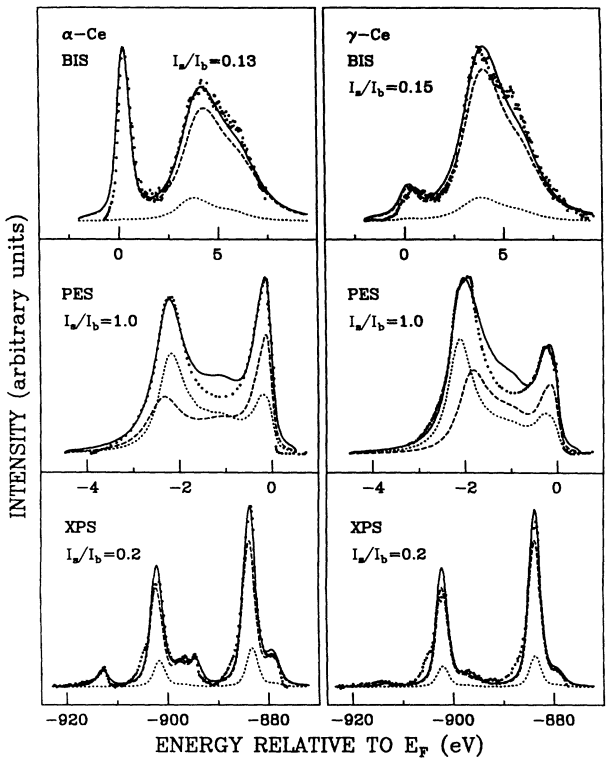

FIG. 3. Comparison of calculated (solid lines) and experimental (dotted lines) $4f$ PES/BIS and $3d$ XPS spectra of α- and γ-Ce. Surface and bulk contributions are indicated with dotted lines and dashed lines, respectively. The I_s/I_b values are indicated for each spectrum.

IV. SURFACE EMISSION AND FITTING PROCEDURE

The surface to bulk emission ratio I_s/I_b is a function of the electron escape depth λ, the thickness of the surface emission layer a, and the electron emission angle relative to the sample surface normal θ as[20]

$$\frac{I_s}{I_b}=\exp(a/\lambda\cos\theta)-1\ . \tag{4}$$

Since this ratio depends on λ, it varies strongly with the electron kinetic energy[21] and changes for different materials. In the rare-earth series, it has been shown that surface sensitivity generally increases with increasing atomic number.[22] Using this information, we have estimated the I_s/I_b ratio at our $4f$ PES kinetic energy (40 ~ 60 eV) to be in the range of 0.5 to 1.5, and used the empirical escape depth curve[21] to extrapolate the I_s/I_b value to higher kinetic energies for the $3d$ XPS (~600 eV for an Al K_α source) and BIS (~1487 eV for Al $K\alpha$ energy photons) spectra. Figure 4 shows the escape depth as a function of the electron kinetic energy. The solid lines are the upper and lower bounds of the empirical escape depth curve for heavy metals.[21] The open circles are escape depths for the rare earths taken from Ref. 22, assuming $a/\cos(\theta)=2.2$ Å in Eq. (4). For an average electron emission angle of $\theta=20°$, typical for most electron analyzers and experimental situations, this corresponds

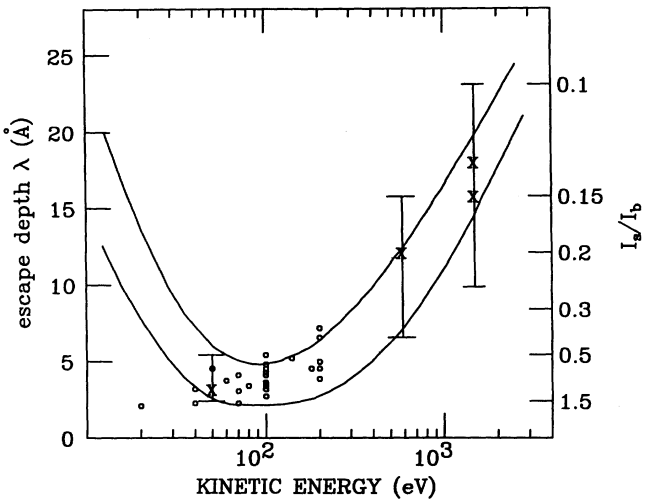

FIG. 4. Escape depth and surface to bulk emission ratio as a function of the electron kinetic energy. The upper and lower bounds are empirical curves for heavy metals taken from Ref. 21, and the open circles are from rare-earth metals (Ref. 22). $a/\cos(\theta)$ is assumed to be 2.2 Å [Eq. (4)]. The vertical lines indicate the estimate of the I_s/I_b ratio used in our analysis for the three spectroscopies. X marks the values used in the fitting of Fig. 3.

to a surface emission layer of $a \sim 2$ Å, about half of the lattice spacing. We notice that the lattice constants among the rare-earth metals change by only about 5%, so that the use of a single a value is reasonable. This places most of the points for rare earths in the range of the empirical escape depth curve, and the Ce data are near the top of the points. The figure also marks the I_s/I_b scale on the right-hand side. At Ce $3d$ XPS kinetic energies, we estimate I_s/I_b to be within 0.15 and 0.4 as shown by the vertical bars in the figure, allowing some uncertainty in choosing $a/\cos(\theta)$.

The ideal method of separating the surface and bulk emission is to have at least two spectra taken at different electron kinetic energies for each one of the the three spectroscopies, and then to scale and subtract the two measured spectra according to the I_s/I_b ratios determined from the escape depth curve. However, for the BIS and $3d$ XPS, such spectra taken at two electron energies do not exist, and for the $4f$ PES the difference in electron energies and thus the I_s/I_b ratios for existing spectra is too small. In this work we make the assumption that the Hamiltonian parameters for all three spectroscopies are the same. As described below, this assumption allows us to separate the surface and bulk contributions, using the fact that the data for the three spectroscopies involve different electron kinetic energies that are well separated from each other and hence have different I_s/I_b ratios. In making this assumption we are ignoring theoretical arguments[10] that the different final-state f and core-hole configurations reached in the three spectroscopies can lead to slightly different values of the hybridization matrix element V. We note, however, that the assumption is quite restrictive in that we must determine the parameters self-consistently, and there is no guarantee in advance that this is possible.

The following self-consistent procedure is used to fit our spectra. In addition to the assumption that the bulk and surface Hamiltonian parameters ε_f, κ, U_{fc}, and U are the same for the different spectroscopies, we also assume that the difference in the bulk and surface parameters is in ε_f and κ only. We first ignore the surface emission contribution in $3d$ XPS and the bulk parameters are adjusted to fit this spectrum. These bulk parameters from $3d$ XPS are then used to calculate the bulk PES spectrum. For a fixed PES I_s/I_b ratio there is only one pair of surface ε_f and κ that can fit the position and relative intensity of the PES "2-eV peak." The newly obtained surface parameters are then used as input for the XPS fit for a given XPS I_s/I_b value, which gives a new set of bulk parameters. After two to three iterations the parameters obtained from consecutive iterations become consistent. For a given I_s/I_b value for $3d$ XPS, and for the surface parameters needed to fit the PES spectra with $I_s/I_b = 0.5$ to 1.5, the surface $3d$ XPS spectrum remains almost unchanged so that only one set of bulk parameters and a range for the surface parameters are obtained. If we allow the $3d$ XPS I_s/I_b value to be within the range specified in Fig. 4, we then get a range for both the surface and the bulk parameters.

For the BIS spectrum, we use the final self-consistent bulk and surface parameters from $3d$ XPS and $4f$ PES, and vary the I_s/I_b ratio in order to fit these spectra. The I_s/I_b values obtained, plotted in Fig. 4, are well within the range of the empirical escape depth curve.

V. RESULTS AND DISCUSSIONS

The various panels of Fig. 3 show an example of the comparison between theoretical (solid lines) and experimental (dots) (Refs. 13–15) $4f$ PES/BIS and $3d$ XPS spectra of α- and γ-Ce. The I_s/I_b values used in the fitting are given in the figure, and are marked with X in Fig. 4 for the three spectroscopies. In each case, the theory curve has been broadened using a Gaussian and Lorentzian function to stimulate the experimental resolution and final-state lifetime effects, respectively. The experimental resolutions for the spectra are full width at half maximum (FWHM) $= 2\Gamma_G = 0.4$ eV for α-Ce BIS, 0.65 eV for γ-Ce BIS, 0.12 eV for α-Ce PES, 0.15 eV for γ-Ce PES, and 0.25 eV for $3d$ XPS. The Lorentzian broadening is FWHM $= 2\Gamma_L = 0.23|E - E_F|$ eV for BIS, $0.1 + 0.17|E - E_F|$ eV for PES, and 2.27 eV for $3d$ XPS. In addition to the lifetime, the $3d$ XPS Lorentzian broadening given here also includes additional broadening to simulate the multiplet splitting. A quadratic energy dependence for the lifetime broadening in the PES/BIS spectra gives almost equally good fits, except that in the BIS spectrum a shoulder at about 5.5 eV due to multiplets becomes slightly smaller.

Similar to earlier findings on $CeIr_2$, $CeRu_2$, and CeAl,[8] but here with data of much better experimental resolution, a nonzero lifetime broadening at the Fermi level is necessary to reproduce the width of the Kondo resonance peak in the $4f$ PES spectra. The origin of this is not

clear, but a possible contribution is a lattice effect in which the Kondo peak has a dispersion. Angle-resolved photoemission on γ-Ce (Ref. 23) with a resolution of 0.3 eV did not show any dispersion, and a better resolution of less than 0.1 eV is needed to test this hypothesis. This extra broadening also causes the smooth turn-on of the theory curve at the Fermi level and a small amount of extra weight is moved to beyond E_F, but this is not numerically significant because the resolution broadening is slightly greater than this extra broadening. In the BIS spectra, because of its lower resolution, we cannot decide whether an extra broadening is necessary.

The inelastic background and the conduction electron (sp) contribution to the raw BIS spectra of Fig. 2, approximated by a straight line with a step turn-on at E_F and broadened with experimental resolution, has been removed. In order to account for loss structures in the $3d$ XPS data, the theory has been convolved with an experimental electron-energy-loss spectrum,[24] resulting in much better comparison between theory and experiment than the step function approximation to the loss spectrum used in Fig. 2. Almost all the features of the various spectra are reproduced by the theory, except that in the experimental $3d$ XPS spectra, there are structures arising from multiplet splittings of the $3d^9 4f^1$ peaks in the spectrum, and these splittings are not included in the theory.

Table I summarizes the parameters obtained from our fits to α- and γ-Ce spectra. The f-level spin-orbit splitting $\Delta\varepsilon_f$ is 0.28 eV, determined from the high-resolution PES data, as shown in detail later. The parameter Δ is the average of $\pi|V(\varepsilon)|^2$ over the energy range 3 eV below E_F. The Hamiltonian parameters from spectral fits were used to calculate[6,7] the zero-temperature susceptibility $\chi(0)$, the singlet ground-state energy E_{gs}, and the Kondo temperature T_K. These quantities are also shown in the table. E_{gs} is measured relative to the f^1 state, and T_K is defined using[25]

$$\chi(0)=C\frac{1-w(f^0)}{T_K}\ , \tag{5}$$

where C is the Curie constant for the lowest-energy $4f$ spin-orbit splitting state $j=\frac{5}{2}$, and $w(f^0)$ is the occupation of the f^0 states. Equation (5) is valid in the first-order calculation with finite U value, and we use it as an ansatz to define T_K in the second-order calculation.

As is by now well appreciated, the main difference between the α- and γ-Ce Hamiltonian parameters is the strength of the hybridization, due to the different lattice constant. This is reflected spectroscopically in the size of the Kondo resonance peak in the $4f$ PES/BIS spectra shown in Fig. 3, and the difference in the f-level occupation, n_f of the two phases. But for both phases, n_f is still close to 1, and this places both α and γ phases in the Kondo regime of the Hamiltonian where $n_f \geq 0.8$.

Also shown in Table I is the rescaling factor κ for the calculated hopping matrix element $V(\varepsilon)$ [Eq. (3)]. This factor for Ce metals is fairly close to 1 compared to

TABLE I. Hamiltonian parameters and ground-state properties obtained from spectral fits. The U values used for BIS fits are 5.34 and 5.44 eV for the α and γ phases, respectively, slightly smaller than the ones used for $3d$ XPS and $4f$ PES as indicated in the table. The $\pm$ values reflect the parameter ranges described in the text. The surface T_K value is the average of the limiting T_K values implied by the limiting $\chi(0)$ values.

		α-Ce	γ-Ce
bulk	ε_f (eV)	-1.27 ± 0.04	1.27 ± 0.04
	Δ_{av} (meV)	66.3 ± 2.0	32.2 ± 0.4
	κ	0.868 ± 0.013	0.844 ± 0.04
	U (eV)	6	6
	U_{fc} (eV)	9.77	9.77
	n_f	0.861 ± 0.015	0.971 ± 0.006
	n_{f0}	0.1658 ± 0.0148	$0.0426\pm0.005\,4$
	n_{f1}	0.8079 ± 0.0151	$0.9444\pm0.000\,5$
	n_{f2}	0.0264 ± 0.0003	$0.0131\pm0.000\,05$
	$\chi(0)$ (10^{-3} emu/mole)	0.70 ± 0.10	8.0 ± 1.4
	T_K (meV)	81.5 ± 12.2	8.2 ± 1.5
	$E_{g.s.}$ (meV)	270 ± 20	122 ± 12
surface	ε_f (eV)	-1.75 ± 0.15	-1.73 ± 0.18
	κ	0.57 ± 0.11	0.76 ± 0.13
	n_f	1.0011 ± 0.0206	0.9993 ± 0.0148
	n_{f0}	0.0126 ± 0.0081	0.0125 ± 0.0007
	n_{f1}	0.9737 ± 0.0122	0.9757 ± 0.0094
	n_{f2}	0.0137 ± 0.0042	0.0118 ± 0.0027
	$\chi(0)$ (10^{-3} emu/mol)	69.1 ± 51.9	50.9 ± 32.1
	T_K (meV)	2.2 ± 1.6	2.2 ± 1.4
	$E_{g.s.}$ (meV)	95.7 ± 34.5	87.3 ± 24.8
	surface f-level shift (eV)	-0.48 ± 0.16	-0.46 ± 0.18
	$\chi(0)$ ($\times10^{-3}$ emu/mole)	0.53 (Ref. 28)	$\sim$4.3 (see text)

$\kappa=0.67$ for $CeCu_2Si_2$ (Ref. 26) and $\kappa=0.707$ for $CeRu_2$.[9] This renormalization could to some extent be due to the orbital dependence of $V(\varepsilon)$ [the vm index in Eq. (1)], but more importantly, it could be that the LDA approximation gives f states that are too extended. The unphysical interaction of the f electron with itself in the LDA would make the potential not sufficiently attractive, resulting in an extended f orbital and increasing the calculated hybridization.

The experimental $\chi(0)$ value in the table for the α phase is from Ref. 27. Because $\chi(0)$ is not directly observable for the γ phase, the value given in the table has been deduced from the quasielastic linewidth Γ in neutron scattering,[28-31] using the theoretical result[32] that for the temperature of interest $\Gamma \approx T_K$. The calculated $\chi(0)$ value is within a factor of 1.1 and 1.5 of the experimental value for the α and γ phases, respectively. It is important to note, however, that the calculated $\chi(0)$ values are always larger than the experimental ones, or, equivalently, the hybridization values from spectroscopy fits are always smaller than those required to reproduce the observed susceptibility values. A possible explanation, discussed elsewhere in detail,[33] is that the Coulomb interaction between the f electrons and the conduction electrons (mostly $5d$) tends to renormalize the hopping matrix element $V(\varepsilon)$ in such a way that $V(\varepsilon)$ is enhanced mostly near $\varepsilon \sim E_F$. In the AIH, thermodynamic properties such as $\chi(0)$ are essentially determined by the value of $V(\varepsilon)$ close to E_F, while electron spectra are influenced by $V(\varepsilon)$ over a larger energy scale. This renormalization effect is, therefore, consistent with our finding that the electron spectra give smaller effective hybridization values. Because of the exponential relation between hybridization and $\chi(0)$, small renormalization of Δ leads to large changes in $\chi(0)$. The fact that our calculated $\chi(0)$ from spectroscopy parameters are in quite good agreement with the experimental value indicates that the renormalization to $V(\varepsilon)$ is not very large.

For both the α and γ phases, the surface $4f$ level is shifted by ~ -0.47 eV relative to the bulk level, consistent with the findings for other rare-earth metals,[22] and the surface hybridization is reduced by factors of $(\kappa_s/\kappa_b)^2=0.44$ and 0.81 relative to the bulk value, for α and γ phases, respectively. Both effects tend to make the surface n_f closer to 1. It is interesting to note from Fig. 3 that the surface ionization peak at ~ 2 eV appears at a smaller binding energy relative to the bulk peak in the α phase, while in the γ phase it appears at a larger binding energy than the bulk peak. This is due to the difference in the hybridization values of the two phases.

In considering the theoretical fits of this paper, it is important to note that good fits are obtained for the PES spectral weight in the first 600 meV below E_F even though this weight greatly exceeds that which would be expected in the simplest theories of the resonance, which take U to be infinite and neglect the spin-orbit splitting of the f^1 state. This is especially true for γ-Ce where T_K is relatively small, and even more so for materials with very small values of T_K, such as CeAl.[8] The origin of this weight is twofold. First, the spin-orbit splitting of the f^1 state gives rise to a sideband structure on the Kondo resonance, at the spin-orbit energy near -0.3 eV. That this sideband can have much more weight than the Kondo resonance itself has been discussed pedagogically in Refs. 1 and 8. Second, as pointed out in Refs. 1 and 8, and discussed in great detail in Ref. 7, the presence of even a small admixture of f^2 states into the ground state gives rise to $f^2 \rightarrow f^1$ photoemission channels which greatly enhance the weight very near E_F, as well as in the sideband region. Certain constructive interference processes are partly responsible for the large effect. The theoretical PES curves for the surface emission show the remarkable magnitude of this extra weight very clearly. Note that T_K is only ~ 2 meV for the surface spectra, but that they nonetheless have in the first 600 meV of binding energy a spectral weight which is an easily observable fraction of the total weight below E_F. In a model with infinite U and no spin-orbit splitting, but parameters adjusted to give the same small T_K, the weight near E_F would be negligible. As discussed next, the theoretical fits are very good not only for th total amount of weight in the low-resolution spectra of Fig. 3, but also for the details of its shape as measured in higher resolution spectra.

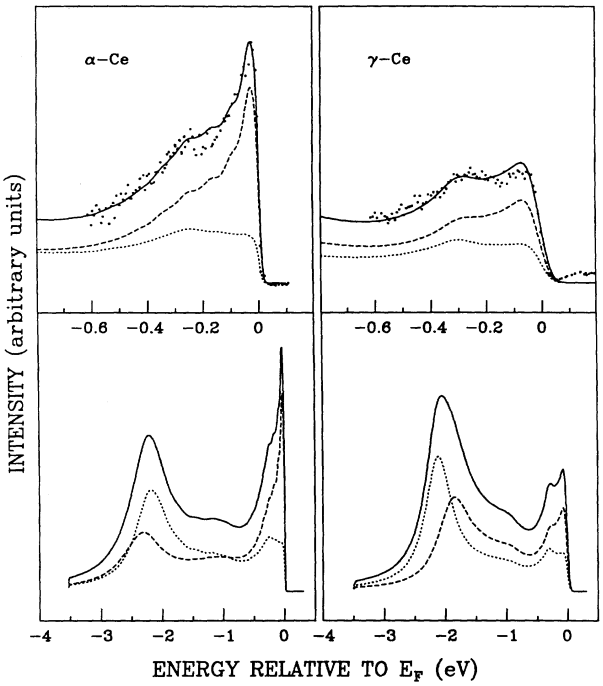

FIG. 5. Top: Calculated (solid lines) and experimental (dotted lines) high-resolution $4f$ PES spectra (Ref. 16) of α- and γ-Ce within 600 meV below E_F. The same set of Hamiltonian parameters is used as in Fig. 3. Surface and bulk contributions are indicated with dotted lines and dashed lines, respectively, and $I_s/I_b=1.0$ for both phases. Bottom: The same theoretical spectra as in the top, but plotted in the entire valence-band region. High-resolution experimental spectra over such a wide binding-energy range are not available.

The highest-resolution $4f$ PES spectra,[16] extracted from spectra taken at photon energy 40.8 and 20.2 eV, are available only for the binding-energy range of 0 to 600 meV below E_F. These spectra are compared with the calculated spectra in Fig. 5. This high-resolution calcula-

tion is performed using exactly the same set of bulk and surface Hamiltonian parameters as in the lower-resolution $4f$ PES spectra of Fig. 3. The little wiggles in the -0.4 to -0.1 eV region of the calculated spectrum for α-Ce are due to the finite energy grid size used in our calculation. The experimental resolution of 20 and 60 meV (Ref. 16) is simulated by a Gaussian broadening for the α and γ phases, respectively. As mentioned earlier, the nonzero lifetime Lorentzian broadening at E_F moves some weight beyond E_F. For these high-resolution spectra this results in a Fermi level that is obviously too broad compared with the experimental data. The following scheme is used to avoid this. The spectrum before broadening $S_0(\varepsilon')$ is convolved according to

$$S(\varepsilon)=\int_{-\infty}^{E_F}\frac{a(\varepsilon')}{\pi}\frac{\Gamma(\varepsilon)S_0(\varepsilon')}{(\varepsilon-\varepsilon')^2+\Gamma(\varepsilon)^2}d\varepsilon' , \tag{6}$$

where

$$\Gamma(\varepsilon)=\begin{cases}0.02+0.085\varepsilon & \text{for } \varepsilon\le 0\\ 0 & \text{for } \varepsilon>0.\end{cases}$$

$a(\varepsilon')$ is chosen so that the integral of the integrand with $S_0(\varepsilon')=\delta(\varepsilon')$ is 1 for any ε' value. This scheme generates a spectrum with zero weight above E_F and puts the weight that would have spilled over E_F uniformly on the spectrum below E_F. The nonzero broadening at E_F, $\Gamma(0)=0.02$ eV, is determined by the width of the main Kondo resonance peak in the α phase. This value is smaller than the broadening needed for the low-resolution spectra of Fig. 3, indicating that there are subtle differences in the two sets of experimental spectra. The structure at ~ -0.3 eV is the spin-orbit sideband of the Kondo peak. The relative weights of the E_F and the Kondo sideband peaks are linked to the hybridization strengths in each of the two phases. For the α phase, the comparison between the data and the calculation is very good. For the γ phase, the E_F peak in the calculated spectrum is slightly larger than the data. The I_s/I_b ratio is assumed to be 1.0 for both phases.

The authors of Ref. 16 have analyzed their high-resolution data to first order in the $1/N$ theory, with an infinite U value, using a semielliptical shape for the hybridization matrix element squared. They obtained $T_K=26$ meV and 5 meV for the α and γ phases, respectively. These parameters are very different from our values (see Table I), and would give $\chi(0)$ values four times larger than the experimental ones, a discrepancy so large that it would invalidate the KVC model of the α-γ transition. The inclusion of surface emission in our fits has the following effects on the Hamiltonian parameters of the bulk. It reduces $|\varepsilon_f|$ and increases $\Delta_{\rm av}$. Moderate changes in these two parameters can have a dramatic effect on the calculated T_K and $\chi(0)$ because of the exponential dependence of T_K and $\chi(0)$ on $|\varepsilon_f|$ and $\Delta_{\rm av}$.[6] As discussed in the previous paragraphs, our calculated ground-state properties are in very good agreement with the experimental ones.

In the $\gamma\rightarrow\alpha$ transition, the hybridization increases due to a decrease in the volume. This results in a larger T_K value for the α phase. In the α phase where temperature $T<T_K$, the magnetic moments are quenched, thus displaying Pauli paramagnetic behavior. For the γ phase, $T>T_K$, and the magnetic moments behave Curie-like. It is important to note the quantitative difference between the Kondo temperature T_K and the ground-state energy $E_{\rm g.s.}$ as shown in Table I. In the case of infinite Coulomb interaction U, these two quantities are identical in the lowest-order calculation. For finite U value, the f^2 states enter the calculation, and causes $|E_{\rm g.s.}|$ to increase, but the effect of the f^2 states on the Kondo temperature T_K is not very large.[25] The impact of these effects on the KVC model is discussed in a companion paper.[18]

Finally, as pointed out already, our analysis ignores the possibility of differences in the Hamiltonian parameters for the three different spectroscopies. The fact that the analysis succeeds self-consistently is evidence that the final-state effects on the parameters are relatively small. Nonetheless, we can anticipate the possibility that when more data is available and analyzed in detail,[34] so that bulk and surface contributions can be separated independently for each spectroscopy, it may be found that the parameters for the three spectroscopies display some differences. We estimate that these differences will not exceed 10–15%, so that the important conclusions drawn here, and in the companion KVC paper,[18] will not be affected.

VI. CONCLUSIONS

To summarize, we have compared and analyzed published electron spectroscopy data for α- and γ-Ce. Including the surface contribution, and by rescaling an energy-dependent hopping matrix element calculated *ab initio* using the LDA approximation, the AIH provides a remarkably good description of the spectroscopy data. The Hamiltonian parameters obtained agree well with the experimental susceptibility $\chi(0)$. Relative to the bulk f states, the Ce surface $4f$ level is shifted by ~ -0.5 eV, and has a reduced hybridization strength. Lattice effects could cause dispersion and thus the additional broadening we find for the Kondo resonance peak in the PES spectrum. We found that a discrepancy between a previous analysis of the high-resolution PES, and the ground-state properties, is eliminated by including the surface emission contribution in the spectral analysis. We conclude that the Anderson impurity Hamiltonian gives a quantitatively unified description of the high-energy spectroscopy and the low-energy properties of α- and γ-Ce metal.

ACKNOWLEDGMENTS

We thank J.-H. Park for suggesting the importance of surface emission, and J. C. Fuggle for giving us permission to use their unpublished energy-loss data. Research support by the U.S. National Science Foundation–Low

Temperature Physics Program, under Grant No. DMR-87-21654 (L.Z.L., J.W.A.) is gratefully acknowledged. Part of this work was performed while J.W.A. was at the Max-Planck-Institut. He thanks Professor O. K. Andersen and Professor P. Fulde and Dr. O. Gunnarsson for hospitality during the visit and gratefully acknowledges the Alexander von Humboldt-Stiftung of the Federal Republic of Germany for supporting the visit.

*Present address: Department of Applied Physics, Yale University, New Haven, CT 06520.

†Present address: Institute of Physics, University of Aarhus, DK-8000 Aarhus C, Denmark.

[1]D. C. Koskenmaki and K. A. Gschneidner, in *Handbook on the Physics and Chemistry of Rare Earths,* edited by K. A. Gschneidner and L. R. Eyring (North-Holland, Amsterdam, 1978), Vol. I, p. 340.

[2]*Narrow Band Phenomena,* edited by J. C. Fuggle, G. A. Sawatzky, and J. W. Allen (Plenum, New York, 1988).

[3]P. W. Anderson, Phys. Rev. **124**, 41 (1961).

[4]J. W. Allen and R. M. Martin, Phys. Rev. Lett. **49**, 1106 (1982); R. M. Martin and J. W. Allen, J. Magn. Magn. Mat. **47&48**, 257 (1985).

[5]O. Gunnarsson and K. Schönhammer, Phys. Rev. Lett. **50**, 604 (1983).

[6]O. Gunnarsson ad K. Schönhammer, Phys. Rev. B **28**, 4315 (1983).

[7]O. Gunnarsson and K. Schönhammer, Phys. Rev. B **31**, 4815 (1985).

[8]J. W. Allen, S.-J. Oh, O. Gunnarsson, K. Schönhammer, M. B. Maple, M. S. Torikachvili, and I. Lindau, Adv. Phys. **35**, 275 (1986).

[9]O. Gunnarsson, N. E. Christensen, and O. K. Andersen, J. Magn. Magn. Mat. **76&77**, 30 (1988).

[10]O. Gunnarsson and O. Jepson, Phys. Rev. B **38**, 3568 (1988).

[11]O. Gunnarsson, O. K. Andersen, O. Jepson, and J. Zaanen, Phys. Rev. B **39**, 1708 (1989).

[12]J. C. Fuggle, F. U. Hillebrecht, Z. Zolnierek, R. Lässer, Ch. Freiburg, O. Gunnarsson, and K. Schönhammer, Phys. Rev. B **27**, 7330 (1983).

[13]E. Wuilloud, H. R. Moser, W.-D. Schneider, and Y. Baer, Phys. Rev. B **28**, 7354 (1983).

[14]D. M. Wieliczka, C. G. Olson, and D. W. Lynch, Phys. Rev. B **29**, 3028 (1984).

[15]F. U. Hillebrecht, J. C. Fuggle, G. A. Sawatzky, and M. Campagna, Phys. Rev. B **30**, 1777 (1984).

[16]F. Patthey, B. Delley, W.-D. Schneider, and Y. Baer, Phys. Rev. Lett **55**, 1518 (1985).

[17]C. Laubschat, E. Weschke, C. Holtz, M. Domke, O. Strebel, and G. Kaindl, Phys. Rev. Lett. **65**, 1639 (1990).

[18]J. W. Allen and L. Z. Liu (unpublished).

[19]R. D. Parks, N. Martensson, and B. Reihl, in *Valence Instabilities,* edited by P. Wachter and H. Boppart (North-Holland, Amsterdam, 1982), p. 239.

[20]M. H. Hecht, A. J. Viescas, I. Lindau, J. W. Allen, and L. I. Johansson, J. Electron Spectrosc. Relat. Phenom. **34**, 343 (1984).

[21]D. A. Shirley, in *Photoemission in Solids I,* edited by M. Cardona and L. Ley (Springer-Verlag, Berlin, 1978), p. 193.

[22]F. Gerken, A. S. Flodström, J. Barth, L. I. Johansson, and C. Kunz, Phys. Scr. **32**, 43 (1985).

[23]E. Jensen and D. M. Wieliczka, Phys. Rev. B **30**, 7340 (1984).

[24]J. C. Fuggle, F. U. Hillebrecht, Z. Zolnierek, R. Lässer, and Ch. Freiburg (unpublished); (private communication).

[25]O. Gunnarsson and K. Schönhammer, in *Theory of Heavy Fermions and Valence Fluctuations,* edited by T. Kasuya and T. Saso (Springer-Verlag, Berlin, 1985), p. 110.

[26]J.-S. Kang, J. W. Allen, O. Gunnarsson, N. E. Christensen, O. K. Andersen, Y. Lassailly, M. B. Maple, and M. S. Torikachvili, Phys. Rev. B **41**, 6610 (1990).

[27]J. M. Lawrence and R. D. Parks, J. Phys. (Paris) Colloq. **37**, C4-249 (1976).

[28]S. M. Shapiro, J. D. Axe, R. J. Birgeneau, J. M. Lawrence, and R. D. Parks, Phys. Rev. B **16** 2225 (1977).

[29]B. D. Rainford, B. Buras, and B. Lebech, Physica **86-88B**, 41 (1977).

[30]C. Stassi, T. Gould, O. D. McMaster, K. A. Gschneidner, and R. M. Nicklow, Phys. Rev. B **19**, 5746 (1975).

[31]A. P. Murani (private communication).

[32]N. E. Bickers, D. L. Cox, and J. W. Wilkins, Phys. Rev. B **36**, 2036 (1987).

[33]O. Gunnarsson and K. Schönhammer, Phys. Rev. B **40**, 4160 (1989).

[34]Such data are now available for the valence-band spectra: E. Weschke, C. Laubschat, T. Simmons, M. Domke, O. Strebel, and G. Kaindl, Phys. Rev. B **44**, 8304 (1991).